Structural Engineering and Mechanics, *Vol. 55, No. 3 (2015) 583-603*
DOI: http://dx.doi.org/10.12989/sem.2015.55.3.583

Modal characteristics of partially perforated rectangular plate with triangular penetration pattern

Myung J. Jhung* and Kyeong H. Jeong[2a]

[1]*Korea Institute of Nuclear Safety, Yuseong-gu, Daejeon, 305-338, Republic of Korea*
[2]*Korea Atomic Energy Research Institute, Yuseong-gu, Daejeon, 305-353, Republic of Korea*

(Received March 1, 2015, Revised May 19, 2015, Accepted June 22, 2015)

Abstract. There are so many applications of perforated pates with various penetration patterns. If they are penetrated regularly, it can be represented by solid plate with equivalent material properties, which has a benefit of finite element modelling and reducing computation time for the analysis. Because the equivalent material properties suggested already are not proper to be applicable for the dynamic analysis, it is necessary to extract the equivalent material properties for the dynamic analysis. Therefore, in this study, the equivalent modulus of elasticity are obtained for the perforated plate with a triangular penetration pattern by comparing the natural frequencies of the perforated plate with those of solid plate, which are represented with respect to the ligament efficacy. Using the equivalent material properties suggested, the modal analyses of the partially perforated rectangular plate with a triangular penetration pattern are performed and its applicability is shown by comparing natural frequencies of perforated and homogeneous solid plates from finite element method and analytical method.

Keywords: partially perforated plate; rectangular plate; effective modulus of elasticity; finite element analysis; Rayleigh-Ritz method; ligament efficiency

1. Introduction

The perforated plates are used widely for various applications in the nuclear industry (Chang *et al*. 2013). To verify the design adequacy it is necessary to perform the finite element analyses due to various dynamic loads such as pump pulsation, random turbulence and earthquake (Ko and Kim 2013, Jhung 1997), and the prerequisite of them is to get the modal characteristics, which needs the finite element model. But if a component have so many holes and especially it is submerged in the fluid, it is time consuming to make a finite element model and it will take a lot of time and need a lot of memory space to perform the analysis (Kim *et al*. 2014, Kerboua *et al*. 2008). Therefore, the concept of equivalent material properties is introduced so that the solid plate is used instead of the perforated one. In this case the equivalent material properties must be defined so as to show the same characteristics between the solid plate with equivalent material properties and perforated plate with original material properties (Cernescu *et al*. 2014).

*Corresponding author, Ph.D., E-mail: mjj@kins.re.kr
[a]Ph.D., E-mail: khjeong@kaeri.re.kr

http://www.techno-press.org/?journal=sem&subpage=8 ISSN: 1225-4568 (Print), 1598-6217 (Online)

The effective elastic constants given by O'Donnell (1973) and Slot and O'Donnell (1971) may be conservatively used for all loading conditions, which is adopted by ASME PVP Code (2007). Using these effective elastic properties, the designer is able to determine the deflections of the perforated sheet for any geometry of application and any loading conditions using available elastic solutions. However the effective elastic constants given by O'Donnell (1973) are not confirmed for the modal analysis of the perforated plate because they are plane stress effective elastic constants based on the in-plane loadings. Jhung and Jeong (2015) developed the coefficients of polynomials for the normalized effective modulus of elasticity of the perforated plate with a square penetration pattern. They also applied them to the partially perforated plate with a square penetration pattern and fixed edges, verifying the adequacy of the suggested equivalent properties by comparing the natural frequencies between finite element analysis and theoretical method.

Therefore, in this study to extend the previous study of Jhung and Jeong (2015), the natural frequencies of the perforated plate with a triangular penetration pattern are obtained as a function of ligament efficiency using finite element analysis. And they are used to extract the effective modulus of elasticity, which is applied to modal analysis of a partially perforated rectangular plate using a homogeneous finite element model. The natural frequencies and the corresponding mode shapes of the homogeneous model are compared with those of the detailed finite element analysis model of the partially perforated plate in order to check the validity of the effective modulus of elasticity.

The suggested effective modulus of elasticity can be applicable to the partially perforated plates to reduce the finite element model size and provide an effective method for dynamic analysis such as modal analysis and seismic analysis based on the finite element method.

2. Theoretical development for natural frequency

To apply the Rayleigh-Ritz approach (Cupial 1997, Ilanko and Monterrubio 2014) to the free vibration analysis of the perforated structure, each mode shape is approximated by a combination of a finite number of admissible functions, $W_{mn}(x,y)$, and an appropriate unknown coefficient, q_{mn}

$$x(x,y,z)=\sum_{m=1}^{M}\sum_{n=1}^{M}q_{mn}W_{mn}(x,y)\exp(i\omega t), \tag{1}$$

where the vector $\boldsymbol{q}$ of the unknown parameters is introduced to perform numerical calculations

$$\boldsymbol{q}=\{q_{11}\ q_{12}\ q_{13}\cdots q_{1N}\ q_{21}\ q_{22}\ q_{23}\cdots q_{MM}\}^{T} \tag{2}$$

A mathematical model of a partially perforated rectangular plate with perforated and solid regions is shown in Fig. 1, where A and B are the width and length of the plate, respectively. The width of peripheral solid region is given as G and the width of the central perforated region is L. The length of peripheral solid region is given as S and the width of the central perforated region is K. The total reference kinetic energy T^{*} of the partially perforated rectangular plate with the thickness of h and the density ρ can be obtained by summation of imperforated peripheral region and central perforated region

$$\boldsymbol{T}^{*}=\frac{h}{2}\boldsymbol{q}^{T}\left[\rho\boldsymbol{Z}_{o}+\left(\rho^{*}-\rho\right)\boldsymbol{Z}_{c}\right]\boldsymbol{q} \tag{3}$$

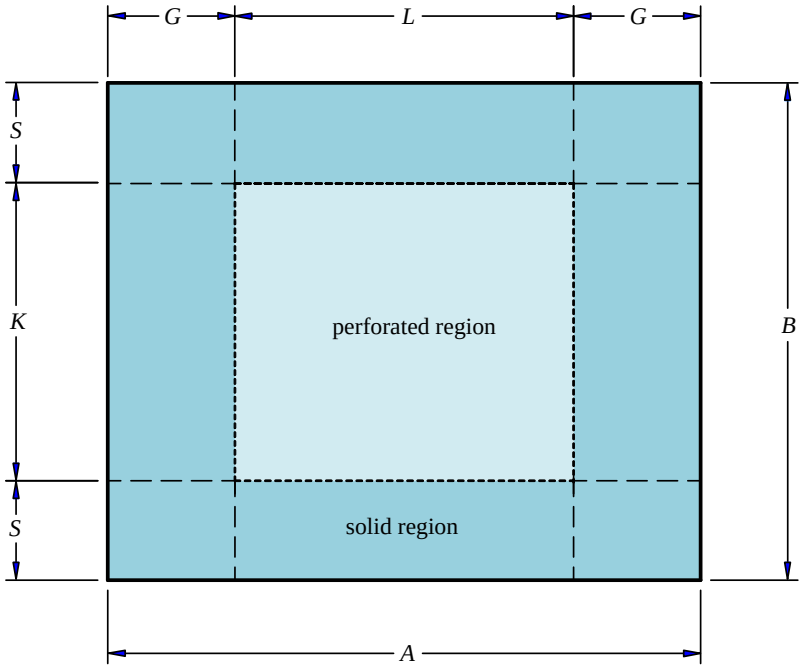

Fig. 1 Partially perforated rectangular plate model

where matrices $\boldsymbol{Z}_O$ and $\boldsymbol{Z}_C$ of Eq. (3) can be defined as

$$\boldsymbol{Z}_o = \int_0^A \int_0^B W_{mn} W_{nv} dy dx = AB, \tag{4}$$

$$\boldsymbol{Z}_c = \int_G^{A-G} \int_S^{B-S} W_{mn} W_{nv} dy dx. \tag{5}$$

Also, the equivalent mass density of the perforated region ρ^* with a triangular penetration pattern can be calculated as

$$\rho^* = \rho \left[1 - \frac{\pi}{2\sqrt{3}} \left(\frac{d}{p} \right)^2 \right] \tag{6}$$

The total maximum potential energy V of the plate can be computed by integrating the derivatives of the admissible modal functions along the imperforated peripheral region and central perforated region

$$V_o = \frac{D}{2} \int_0^B \int_0^A \left[\left\{ \frac{\partial^2 W_{mn}}{\partial x^2} \frac{\partial^2 W_{uv}}{\partial x^2} \right\} + \left\{ \frac{\partial^2 W_{mn}}{\partial y^2} \frac{\partial^2 W_{uv}}{\partial y^2} \right\} \right.$$

$$\left. + \nu \left\{ \frac{\partial^2 W_{mn}}{\partial x^2} \frac{\partial^2 W_{uv}}{\partial y^2} + \frac{\partial^2 W_{uv}}{\partial x^2} \frac{\partial^2 W_{mn}}{\partial y^2} \right\} + 2(1-\nu) \left\{ \frac{\partial^2 W_{mn}}{\partial x \partial y} \frac{\partial^2 W_{uv}}{\partial x \partial y} \right\} \right] dx dy, \tag{7}$$

$$V_c = \frac{D^*}{2}\int_S^{B-S}\int_G^{A-G}\left[\left\{\frac{\partial^2 W_{mn}}{\partial x^2}\frac{\partial^2 W_{uv}}{\partial x^2}\right\}+\left\{\frac{\partial^2 W_{mn}}{\partial y^2}\frac{\partial^2 W_{uv}}{\partial y^2}\right\}\right.$$

$$\left.+\nu\left\{\frac{\partial^2 W_{mn}}{\partial x^2}\frac{\partial^2 W_{uv}}{\partial y^2}+\frac{\partial^2 W_{uv}}{\partial x^2}\frac{\partial^2 W_{mn}}{\partial y^2}\right\}+2(1-\nu)\left\{\frac{\partial^2 W_{mn}}{\partial x\partial y}\frac{\partial^2 W_{uv}}{\partial x\partial y}\right\}\right]dxdy, \tag{8}$$

where D and D^* are the flexural rigidities of the solid and perforated plates, respectively.

Inserting the admissible functions into Eqs. (7) and (8) gives the total maximum potential energy of the partially perforated square plates as a matrix form

$$V = \frac{1}{2}\boldsymbol{q}^T\left[D\boldsymbol{U}_o + (D^* - D)\boldsymbol{U}_c\right]\boldsymbol{q}, \tag{9}$$

where the matrices $\boldsymbol{U}_O$ and $\boldsymbol{U}_C$ can also be derived as

$$\boldsymbol{U}_o = \Delta 1_{mu}\Gamma 2_{nv} + \Delta 2_{mu}\Gamma 1_{nv} + 2\nu\Delta 3_{mu}\Gamma 3_{nv} + 2(1-\nu)\Delta 4_{mu}\Gamma 4_{nv}, \tag{10}$$

$$\boldsymbol{U}_c = \Xi 1_{mu}\Theta 2_{nv} + \Xi 2_{mu}\Theta 1_{nv} + 2\nu\Xi 3_{mu}\Theta 3_{nv} + 2(1-\nu)\Xi 4_{mu}\Theta 4_{nv}, \tag{11}$$

and

$$\Delta 1_{mu} = \int_0^A X_m''(x)\,X_u''(x)dx, \tag{12}$$

$$\Delta 2_{mu} = \int_0^A X_m(x)\,X_u(x)dx, \tag{13}$$

$$\Delta 3_{mu} = \int_0^A X_m''(x)\,X_u(x)dx, \tag{14}$$

$$\Delta 4_{mu} = \int_0^A X_m'(x)\,X_u'(x)dx, \tag{15}$$

$$\Gamma 1_{nv} = \int_0^B Y_n''(y)Y_v''(y)dy, \tag{16}$$

$$\Gamma 2_{nv} = \int_0^B Y_n(y)Y_v(y)dy, \tag{17}$$

$$\Gamma 3_{nv} = \int_0^B Y_n''(y)Y_v(y)dy, \tag{18}$$

$$\Gamma 4_{nv} = \int_0^B Y_n(y)'Y_v'(y)dy, \tag{19}$$

$$\Xi 1_{mu} = \int_G^{A-G} X_m(x)\,X_u(x)dx, \tag{20}$$

$$\Xi 2_{mu} = \int_G^{A-G} X_m''(x)\,X_u''(x)dx, \tag{21}$$

$$\Xi 3_{mu} = \int_G^{A-G} X_m(x)\,X_u''(x)dx, \tag{22}$$

$$\Xi 4_{mu} = \int_{G}^{A-G} X_m'(x)\, X_u'(x)dx, \tag{23}$$

$$\Theta 1_{nv} = \int_{S}^{B-S} Y_n(y) Y_v(y)dy, \tag{24}$$

$$\Theta 2_{nv} = \int_{S}^{B-S} Y_n''(y) Y_v''(y)dy, \tag{25}$$

$$\Theta 3_{nv} = \int_{S}^{B-S} Y_n(y) Y_v''(y)dy, \tag{26}$$

$$\Theta 4_{nv} = \int_{S}^{B-S} Y_n'(y) Y_v'(y)dy. \tag{27}$$

The apostrophe (′) in Eqs. (12) through (27) also indicates a derivative with respect to the corresponding variable. Similarly, minimizing the Rayleigh quotient with respect to the unknown parameters $\boldsymbol{q}$, the Galerkin equation yields

$$[D\boldsymbol{U}_o + (D^* - D)\boldsymbol{U}_c]\boldsymbol{q} - \omega^2 h[\rho \boldsymbol{Z}_o + (\rho^* - \rho)\boldsymbol{Z}_c]\boldsymbol{q} = \{0\}. \tag{28}$$

3. Determination of equivalent material properties

To extract the equivalent modulus of elasticity as a function of ligament efficiency, a perforated square plate with a triangular penetration pattern of holes was examined using the finite element analysis. The geometry and physical properties of a fully perforated square plate model are listed in Table 1.

The configuration of the perforated square plate illustrated in Fig. 2 is used to extract the equivalent material property or effective modulus of elasticity. The number of circular holes in the plate is enough to extract the equivalent properties. The finite element model for the fully perforated square plate with a triangular penetration pattern of holes is shown in Fig. 3. The finite element analysis was carried out using commercial computer software, ANSYS (2013) with Block Lanczos method (Grimes *et al*. 1994, Li and Zhang 2013). The natural frequencies of the perforated plate are normalized with respect to those of imperforated solid plate as a function of the ligament efficiency. The ligament efficiency, η (=(p–d)/p), is defined as the ligament gap divided by the pitch.

Figs. 4 through 6 show normalized natural frequencies of the perforated plate with fixed, simply supported and free edges, respectively. As the flexural rigidity of the plate is reduced

Table 1 Geometry and physical properties of a fully perforated square plate model.

Physical properties in solid condition	Modulus of elasticity	E	69 GPa
	Poisson's ratio	ν	0.33
	Density	ρ	2700 kg/m^3
Geometry	Perforated area	a	384 mm×384 mm
	Circular hole diameter	d	0~15.6 mm
	Pitch	p	16.0 mm
	Thickness	h	3 mm

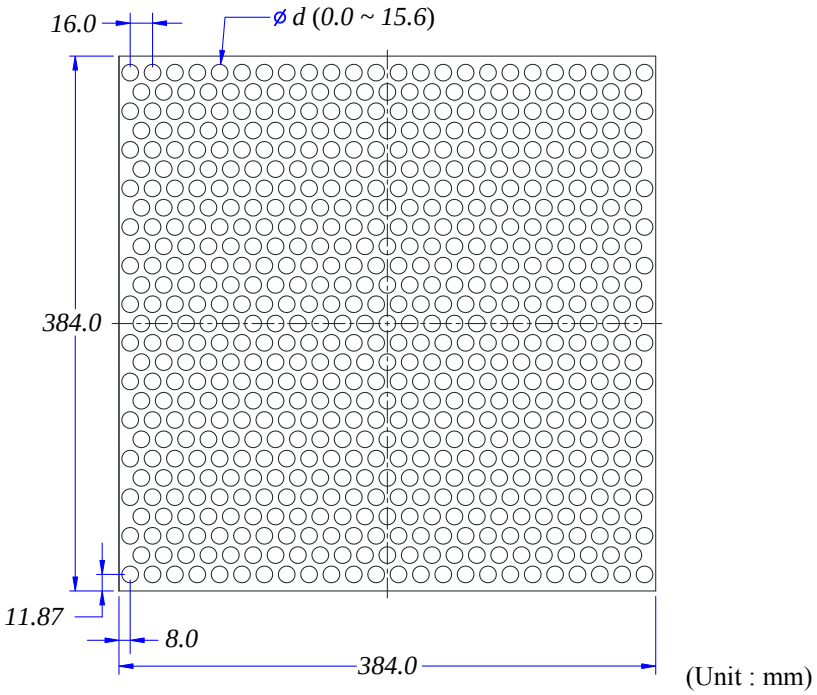

Fig. 2 Perforated square plate model to extract equivalent material properties

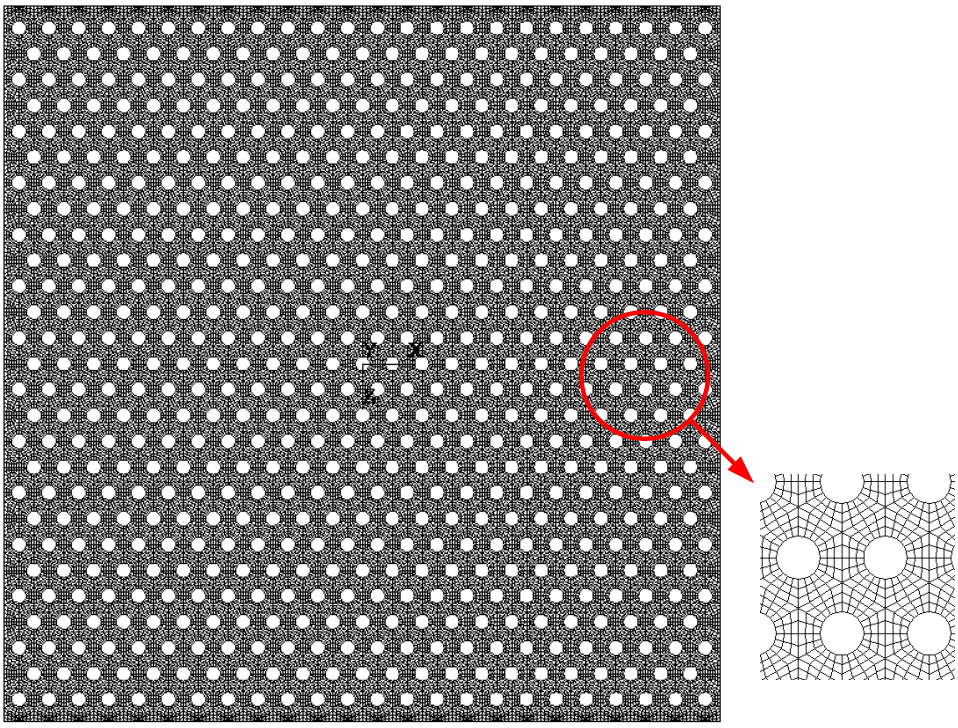

Fig. 3 Typical finite element analysis model of a square plate

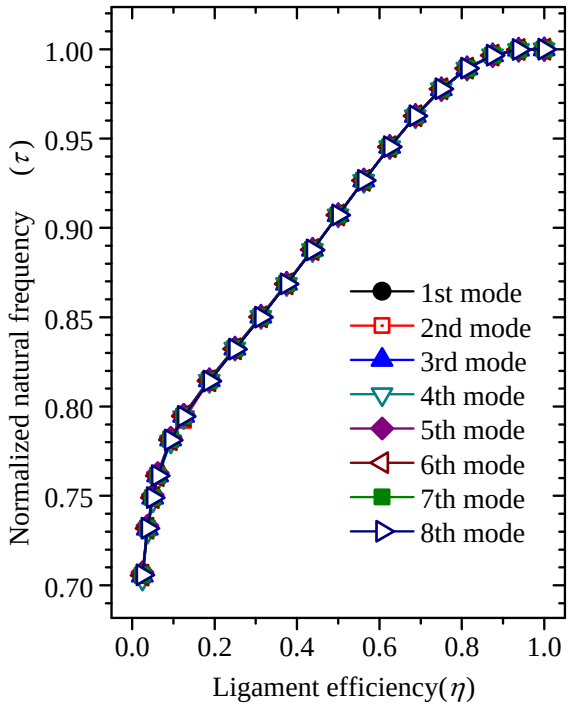

Fig. 4 Normalized natural frequency of a perforated square plate with fixed edges

rapidly and the inertia of the plate is proportionally reduced with the hole area, the normalized natural frequencies are decrease with the hole size. The normalized natural frequencies for the fixed and simply supported cases can be categorized into three regions; the first region between approximately η=0.8 and η=1.0, shows a slow reduction in normalized natural frequencies; the second region between approximately η=0.8 and η=0.2, represents a linear reduction of normalized natural frequencies, finally; the third region, less than η=0.2, reveals an abrupt reduction in normalized natural frequencies.

As a rule, for the fixed case, the normalized natural frequencies of the perforated square plate do not depend on the mode number but the ligament efficiency only as illustrated in Fig. 4. On the contrary, the normalized natural frequencies of the perforated square plate with simply supported and free edges depend on not only the mode number but also the ligament efficiency as illustrated in Figs. 5 and 6. As shown in Fig. 5, the normalized natural frequencies of the perforated square plate with simply supported edges do not depend on the mode number in the higher ligament efficiency, but they spread wide at the narrow ligament range according to the mode numbers.

The first mode normalized natural frequency of the perforated square plate with free edges is linearly reduced slowly from unity to approximately 0.9 in the range of η=1.0 to 0.3, and then it is drastically reduced with a hole size when the ligament efficiency, η is less than 0.3. On the other hand, the third mode normalized natural frequency of the perforated square plate with free edges linearly increase in the range of η=0.1~0.8. The normalized natural frequency of the perforated square plate with the free edges seriously depends on the mode number when the ligament efficiency is less than 0.80. As a consequence, it is needless to say that a fixed effective flexural rigidity cannot exist independently of the plate boundary condition. Therefore, the suggestion of

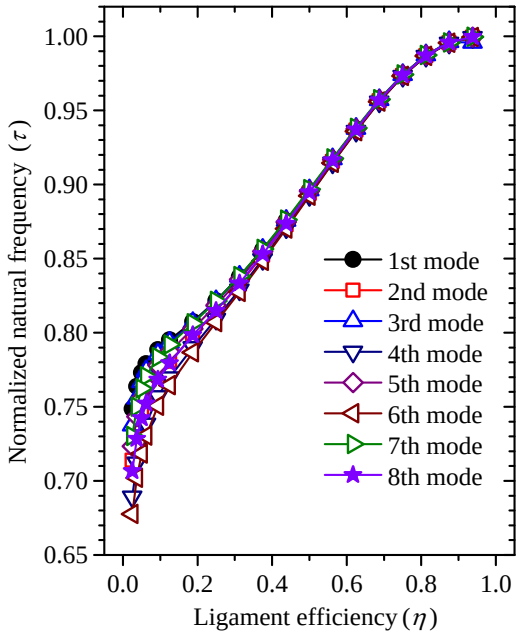

Fig. 5 Normalized natural frequency of a perforated square plate with simply supported edges

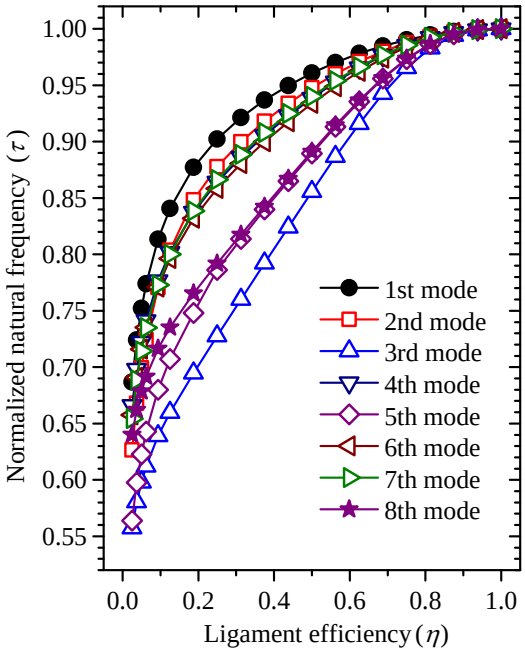

Fig. 6 Normalized natural frequency of the perforated square plate with free edges

O'Donnell (1973) and Slot and O'Donnell (1971), which is adopted by ASME PVP Code, Section III, Division 1, Appendices, Non-mandatory Appendix A (ASME 2007), may lead to inadequate results in dynamic analysis of perforated plates.

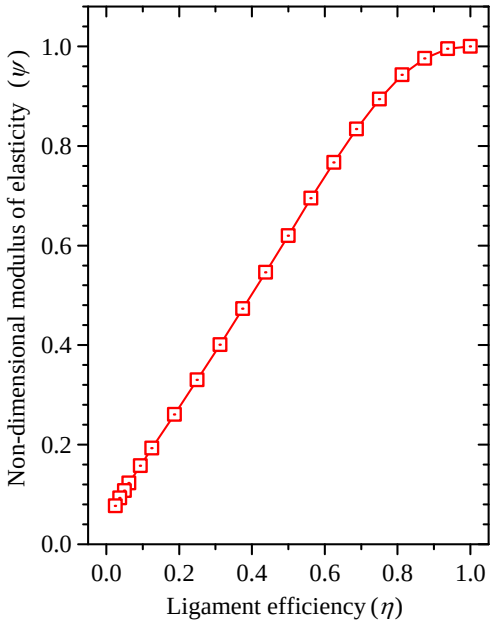

Fig. 7 Effective modulus of elasticity for a perforated square plate with fixed edges

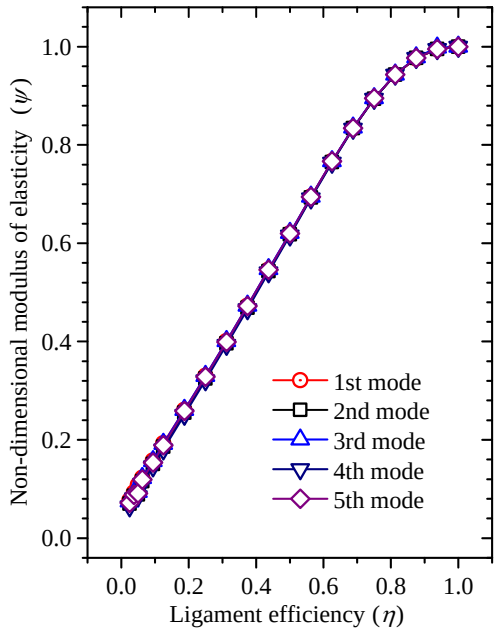

Fig. 8 Effective modulus of elasticity for a perforated square plate with simply supported edges

The effective moduli of elasticity of the perforated plate with a triangular penetration are obtained using an inverse method as shown in Figs. 7 and 8 by defining the equivalent elastic constants such that the modal characteristics of the perforated plate with original properties are the same as those of a solid plate with modified equivalent properties. The effective moduli of

Table 2 Coefficients of polynomials for the normalized effective modulus of elasticity

Boundary condition		Coefficients of polynomials				
		C_0	C_1	C_2	C_3	C_4
Fixed edges		0.03945	1.26910	−0.51685	1.26780	−1.06239
Simply supported edges	1st mode	0.05011	1.17405	−0.51177	1.51015	−1.22555
	2nd mode	0.03929	1.20695	−0.57331	1.58789	−1.26388
	3rd mode	0.03434	1.20832	−0.55733	1.57352	−1.26190
	4th mode	0.05011	1.17405	−0.51177	1.51015	−1.22555
	5th mode	0.05011	1.17405	−0.51177	1.51015	−1.22555

elasticity of the perforated plate with the fixed and simply supported edges approximately do not depend upon the mode number, but they are given as a function of the ligament efficiency. However, the effective modulus of elasticity of the perforated plate with the free edges seriously varies with both the ligament efficiency and mode number. The normalized effective moduli of elasticity, ψ, can be approximated by polynomials given Eq. (29).

$$\psi = C_0 + C_1\eta + C_2\eta^2 + C_3\eta^3 + C_4\eta^4 \tag{29}$$

The coefficients of polynomials for the normalized effective moduli of elasticity are obtained by the curve fitting and listed in Table 2. The coefficients of polynomials obtained by the polynomial curve fitting for the simply supported boundary condition depend on the mode numbers.

The typical mode shapes of the perforated square plate with fixed, simply supported and free edges are shown in Figs. 9 through 11, respectively. The perforation of the plate can change the mode shapes. The 1st, 3rd, 4th, and 8th mode shapes of the perforated square plate with fixed edges are identical to those of the imperforated solid square plate. However, the 2nd, 5th, 6th, 7th, 9th, 10^{th} and 11th mode shapes of the perforated square plate with fixed edges are different from those of the imperforated solid square plate. The distortion in mode shapes of the perforated square plate may cause the boundary rigidity of the plate. Although the square penetration pattern of a square plate can make an identical geometric boundary, the triangular penetration pattern of the square plate cannot make an identical geometric boundary. Therefore, the flexural rigidity in width along the horizontal edges differs from that in length along the vertical edges. It breaks the diagonal symmetry as shown in Figs. 9 and 10.

The 1st, 3rd, 7th and 8th mode shapes of the perforated square plate with simply supported edges are identical to those of the imperforated solid square plate with the same edges. However, the 2nd, 4th, 5th, 6th, 9th, 10th and 11th mode shapes of the perforated square plate with simply supported edges are different from those of the imperforated solid square plate. It also shows that the perforation of the square plate tends to make the nodal line of mode shapes straight as shown in the 2nd, 6th and 11th modes of Fig. 10. The similar results can be observed for the free boundary condition as illustrated in Fig. 11.

4. Results and discussion

The elastic constant extracted previously is checked whether it can be applicable to the partially perforated rectangular plate as shown in Fig. 12 for triangular penetration patterns. The

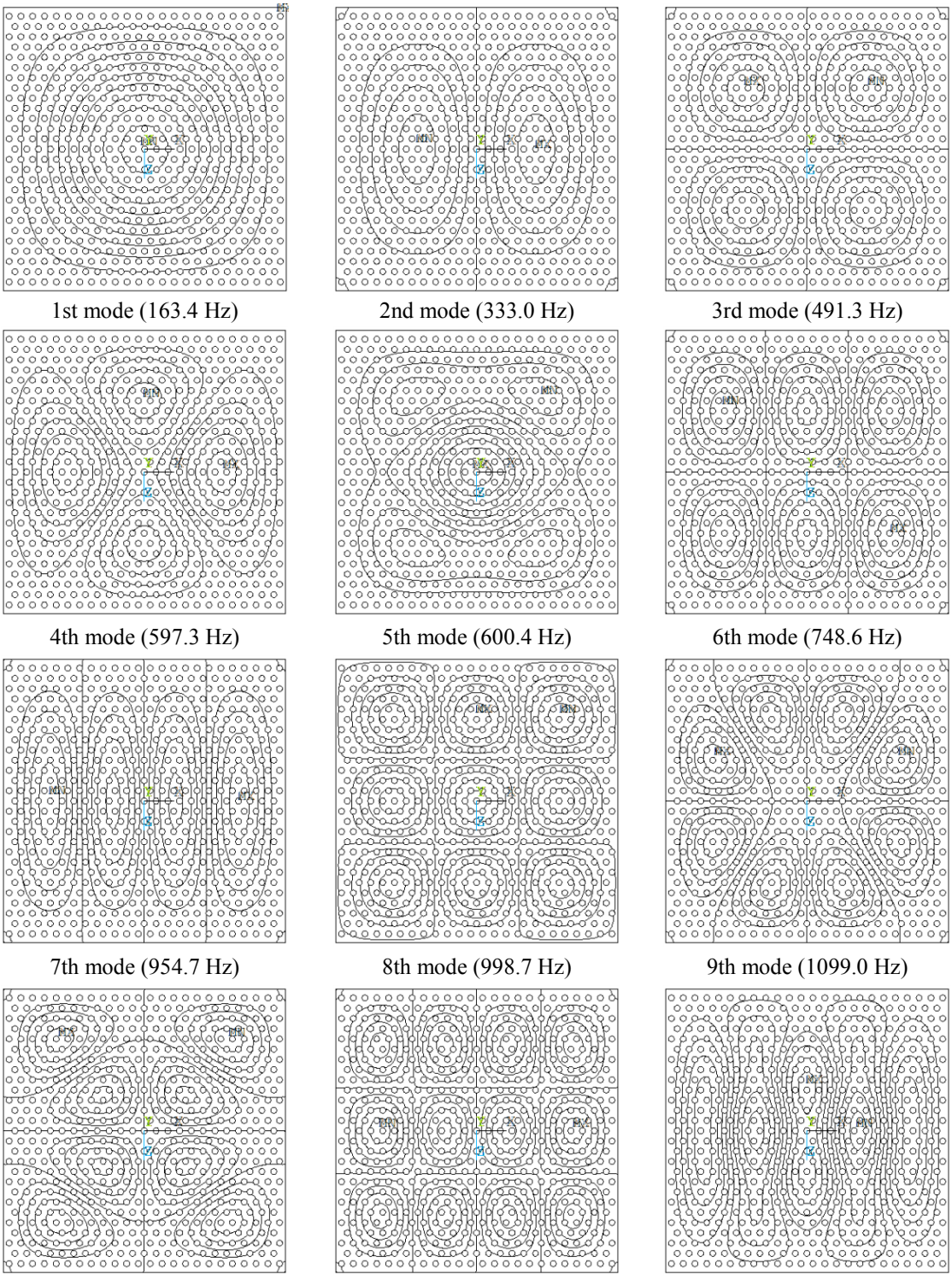

Fig. 9 Typical mode shapes of a perforated square plate with fixed edges

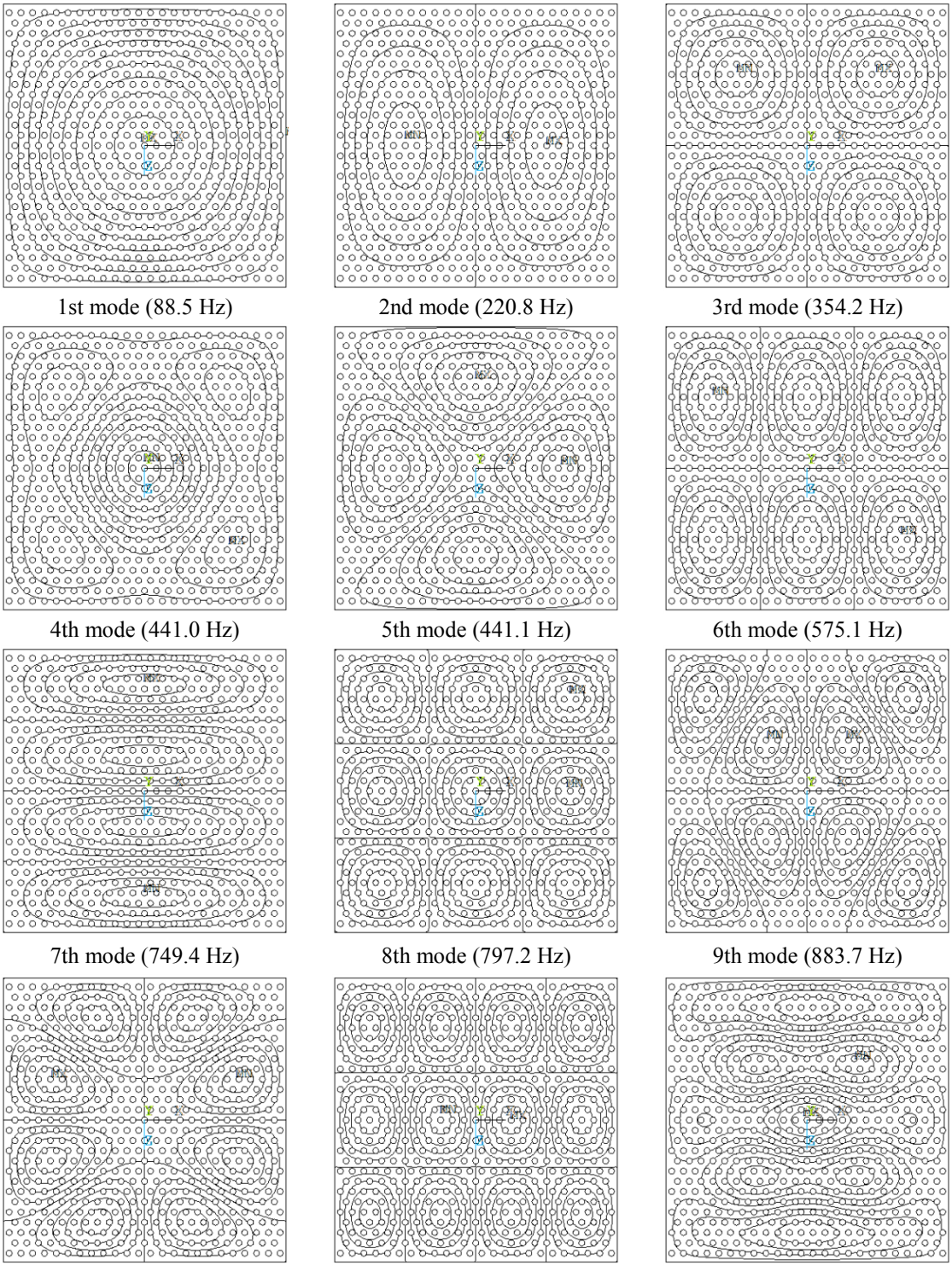

Fig. 10 Typical mode shapes of a perforated square plate with simply supported edges

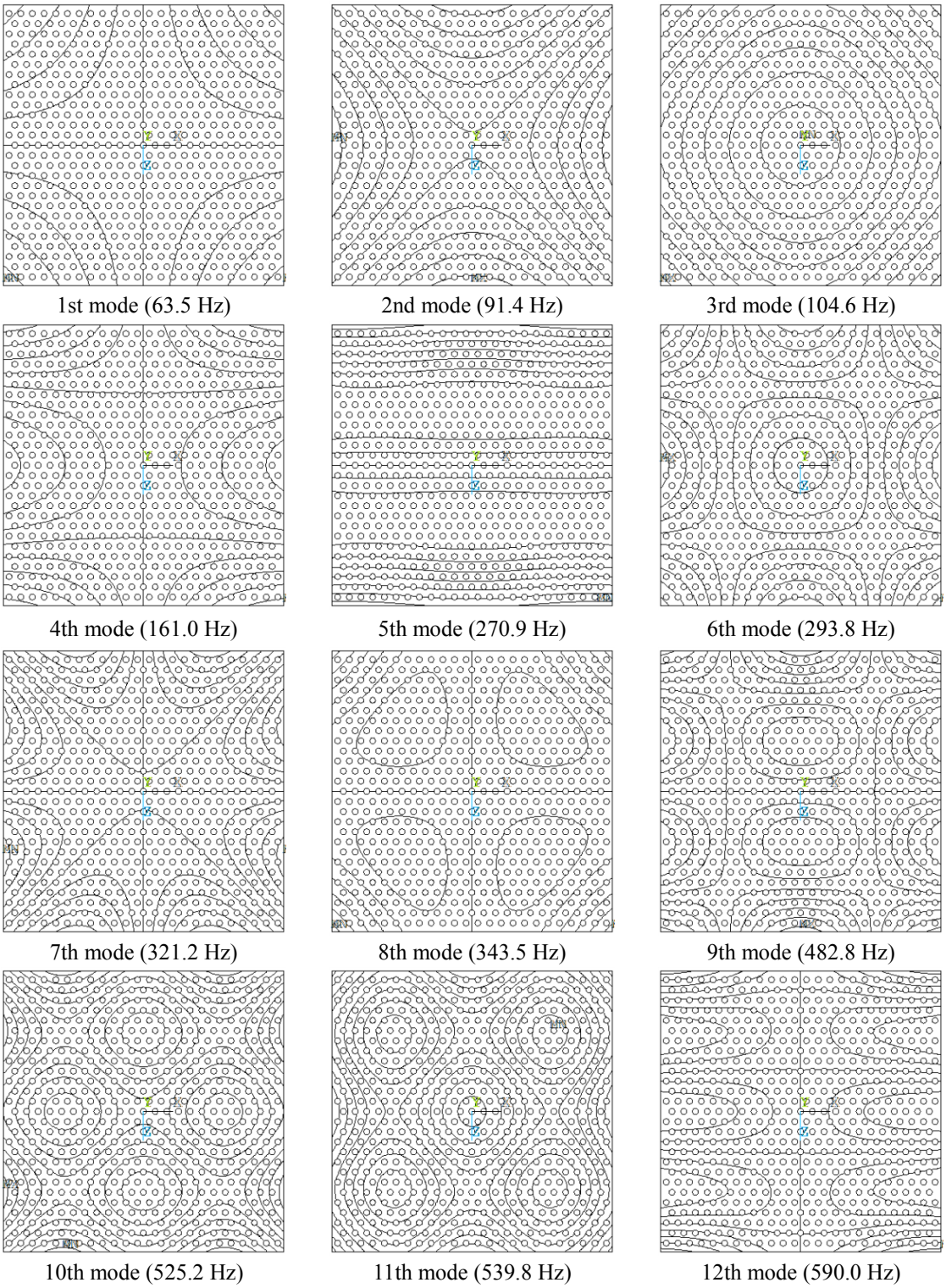

Fig. 11 Typical mode shapes of a perforated square plate with free edges

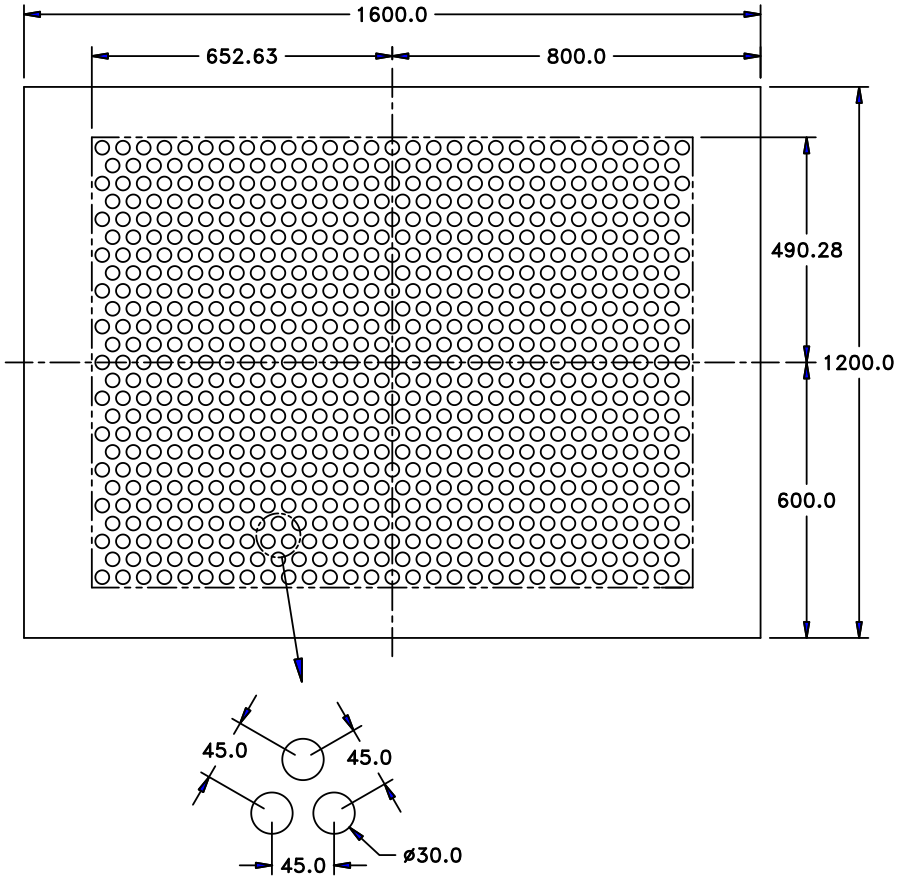

Fig. 12 Model of a partially perforated rectangular plate with a triangular penetration pattern

geometry and material properties are listed in Table 3. The partially perforated plates are assumed as a rectangular plate which is divided into two regions, inner perforated region and peripheral solid region, as shown in Fig. 1. As the inner perforated region can be regarded as a homogeneous plate which has an effective modulus of elasticity and an equivalent mass density, but the outer peripheral solid region has an original modulus of elasticity and mass density (Jhung and Jeong 2015). The effective modulus of elasticity of the inner perforated region is determined by Eq. (29) and the equivalent mass density is calculated by Eq. (6). Finally, the theoretical natural frequencies can be calculated using Eq. (28). Finite element analyses for the partially perforated plates defined by Fig. 12 and Table 3 were performed to confirm the theoretical method characterized by Eq. (28) using ANSYS.

The natural frequencies of the partially perforated rectangular plate are extracted by the suggested theory and two finite element analyses. The results from finite element analysis using effective modulus of elasticity (E^*) are compared with those from finite element analyses of the perforated plate model. It will show validity of the effective modulus of elasticity for the perforated rectangular plate modal analysis. The effective modulus of elasticity calculated by Eq. (29) and the equivalent density (ρ^*) given by Eq. (6) are used in the finite element analysis with the homogeneous model.

Table 3 Geometry and physical properties of a partially perforated rectangular plate model

Physical properties in solid plate	Modulus of elasticity	E	195 GPa
	Poisson's ratio	ν	0.30
	Density	ρ	7770 kg/m^3
Rectangular plate geometry	Total plate area	$A\times B$	1600 mm×1200 mm
	Perforated area	$L\times K$	1305 mm×980 mm
	Circular hole diameter	d	30 mm
	Pitch	p	45 mm
	Thickness	h	8 mm

Table 4 Natural frequencies of a partially perforated rectangular plate with fixed edges

Serial mode number	Natural frequency (Hz)			Discrepancy between FEM results (%)	Discrepancy between theory and FEM result (%)
	Theory	FEM (ANSYS)			
		Perforated model	Homogeneous model		
1	38.56	38.35	38.81	0.55	1.20
2	63.11	62.78	63.73	0.53	1.51
3	88.64	87.70	89.04	1.07	1.53
4	102.8	101.4	103.31	1.38	1.88
5	110.5	109.9	111.95	0.55	1.87
6	147.6	146.3	149.51	0.89	2.19
7	155.5	152.0	155.43	2.30	2.26
8	160.7	159.6	162.34	0.69	1.72
9	181.8	181.1	184.66	0.39	1.97
10	199.3	195.5	200.30	1.94	2.46
11	217.4	214.5	219.31	1.35	2.24
12	220.4	216.4	221.36	1.85	2.29

Table 5 Natural frequencies of a partially perforated rectangular plate with simply edges

Serial mode number	Natural frequency (Hz)			Discrepancy between FEM results (%)	Discrepancy between theory and FEM result (%)
	Theory	FEM (ANSYS)			
		Perforated model	Homogeneous model		
1	19.59	18.93	19.61	3.49	3.59
2	40.87	38.90	40.22	5.06	3.39
3	53.72	52.72	54.19	1.90	2.79
4	74.67	70.51	72.45	5.90	2.75
5	79.64	74.93	77.42	6.28	3.32
6	108.26	108.47	110.96	-0.19	2.29
7	118.92	114.82	117.24	3.57	2.11
8	137.55	131.67	135.29	4.46	2.75
9	159.30	153.58	157.78	3.72	2.73
10	172.72	166.92	171.60	3.47	2.80
11	180.51	172.95	175.93	4.37	1.72
12	182.96	187.08	190.85	4.34	2.02

Tables 4 and 5 show 12 natural frequencies of a partially perforated rectangular plate with fixed and simply supported edges, respectively. The discrepancies between FEM results and theoretical natural frequencies are less than 3%. The discrepancies are greater than those for the simply supported boundary condition. It may be caused by the application of first mode effective modulus of elasticity in the simply supported case. As a result, it is found that the maximum discrepancy between the estimations by the FEM analysis and theoretical results is 6.28% as listed in Table 5. Therefore, the effective modulus of elasticity cannot be recommended in the modal analysis of the partially perforated plate with simply supported edges. However, it is clear that the Rayleigh-Ritz method applying the effective modulus of elasticity and the equivalent density is effective in the analysis of the partially perforated rectangular plate with fixed edges.

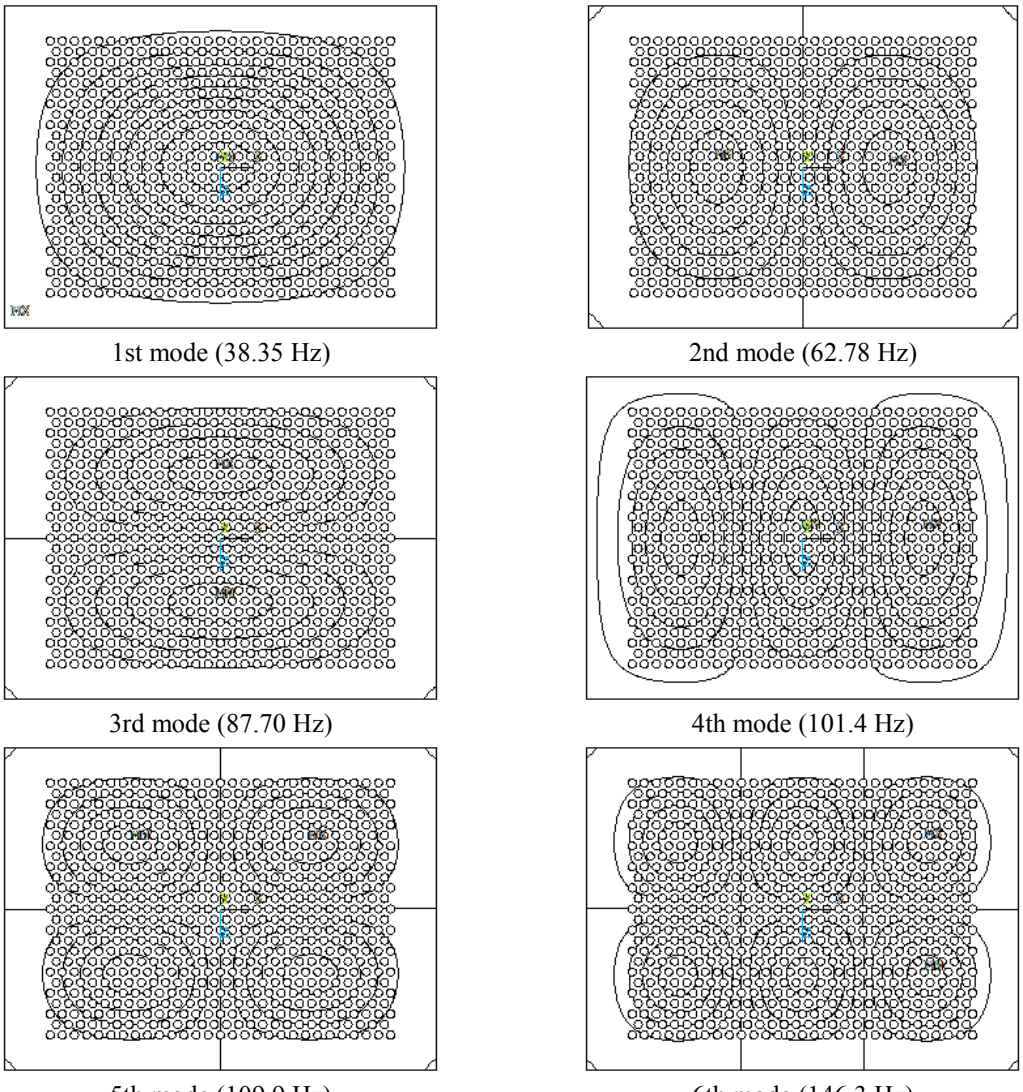

Fig. 13 Mode shapes for a partially perforated rectangular plate with fixed edges

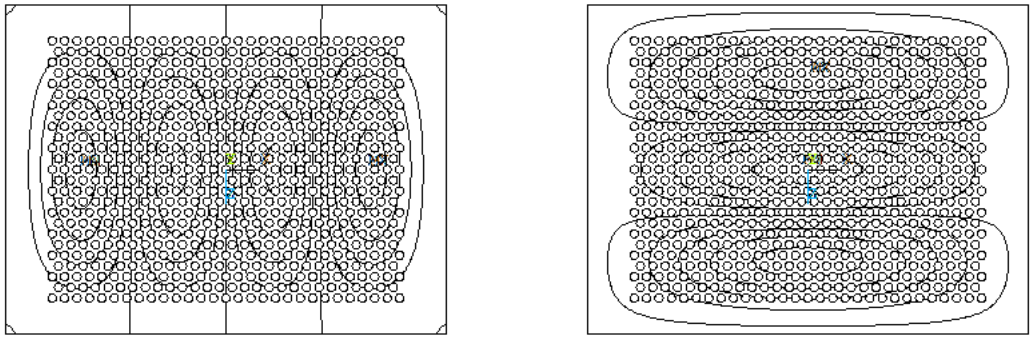

7th mode (152.0 Hz) 8th mode (159.6 Hz)

Fig. 13 Continued

The mode shapes of the rectangular perforated plates with the fixed and simply supported edges, for the full model, are illustrated in Figs. 13 and 14, respectively. The mode shapes of the rectangular perforated plates with the fixed and simply supported edges, for the simplified model using the equivalent material properties, are illustrated in Figs. 15 and 16, respectively. It can be found that the mode shapes of the full model are also preserved in those of the simplified homogeneous model.

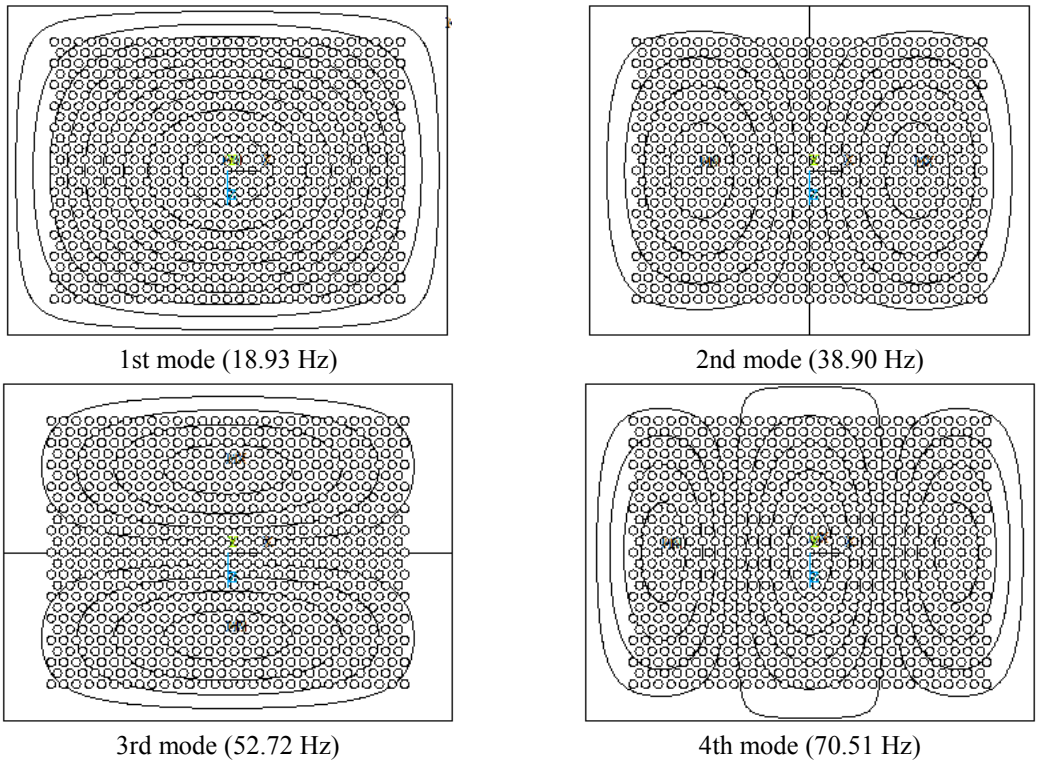

1st mode (18.93 Hz) 2nd mode (38.90 Hz)

3rd mode (52.72 Hz) 4th mode (70.51 Hz)

Fig. 14 Mode shapes for a partially perforated rectangular plate with simply supported edges

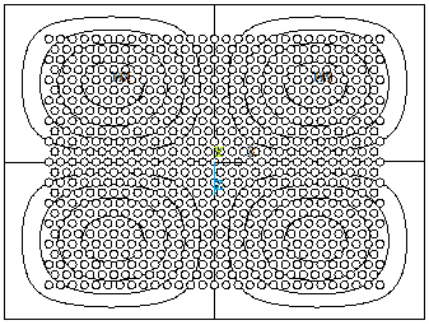

5th mode (74.93 Hz)

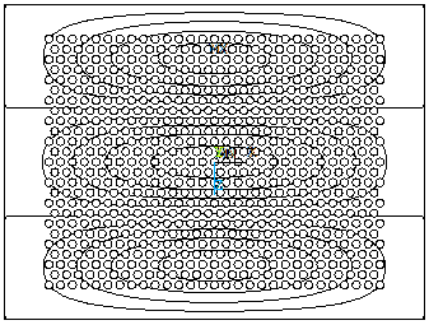

6th mode (108.4 Hz)

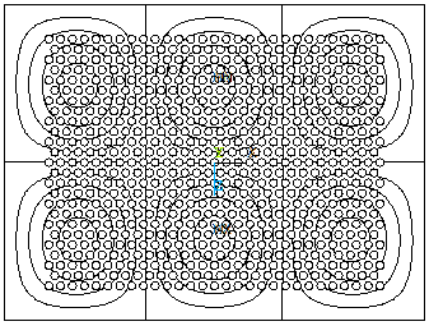

7th mode (114.8 Hz)

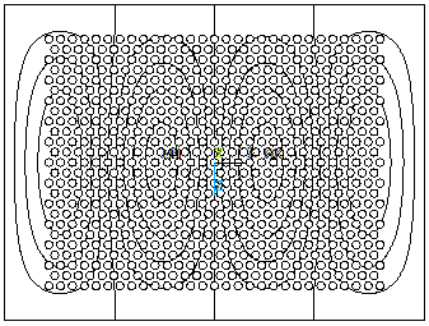

8th mode (131.7 Hz)

Fig. 14 Continued

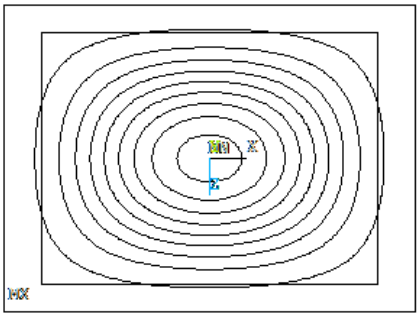

1st mode (38.81 Hz)

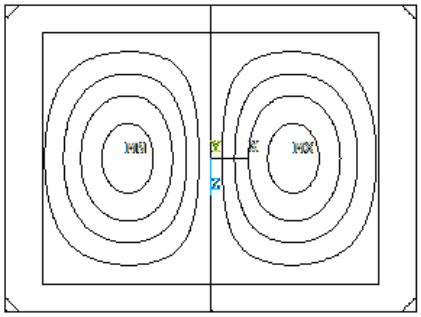

2nd mode (63.73 Hz)

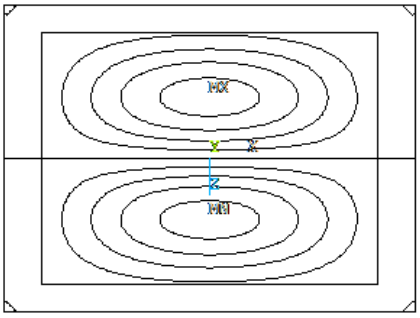

3rd mode (89.04 Hz)

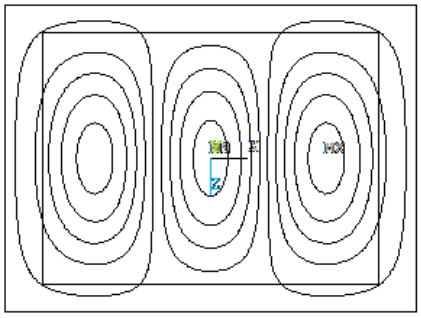

4th mode (103.31 Hz)

Fig. 15 Mode shapes for a partially perforated rectangular plate with fixed edges using equivalent material properties

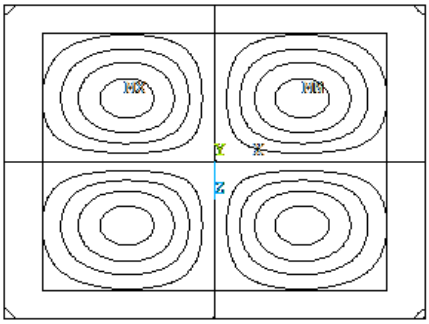

5th mode (111.95 Hz)

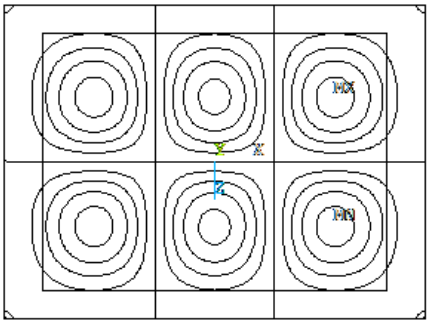

6th mode (149.51Hz)

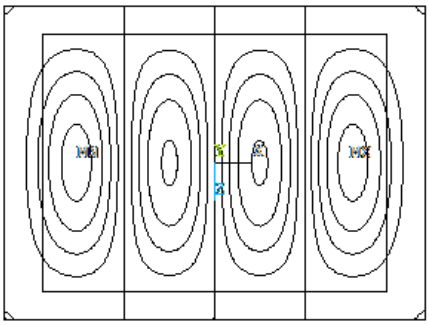

7th mode (155.43 Hz)

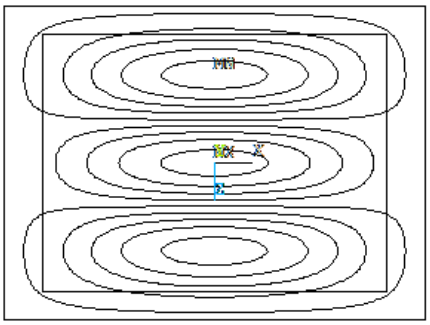

8th mode (162.34 Hz)

Fig. 15 Continued

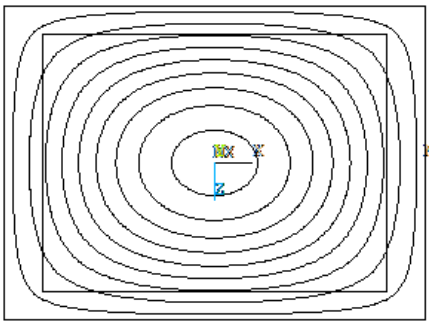

1st mode (19.61 Hz)

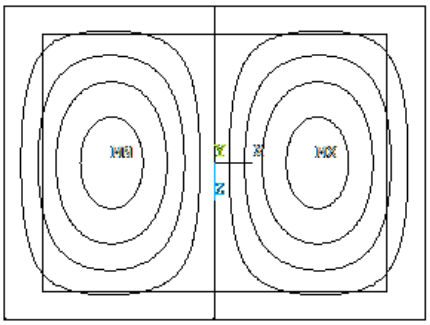

2nd mode (40.22 Hz)

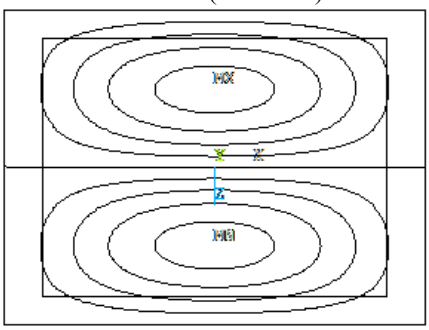

3rd mode (54.19 Hz)

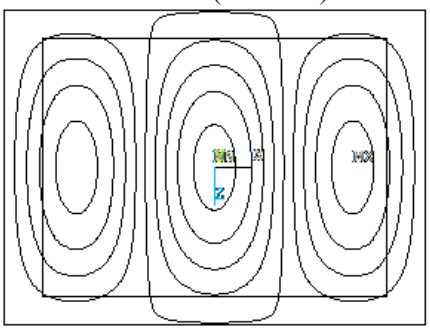

4th mode (72.45 Hz)

Fig. 16 Mode shapes for a partially perforated rectangular plate with simply supported edges using equivalent material properties

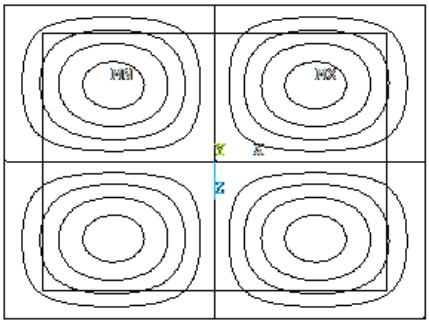

5th mode (77.42 Hz)

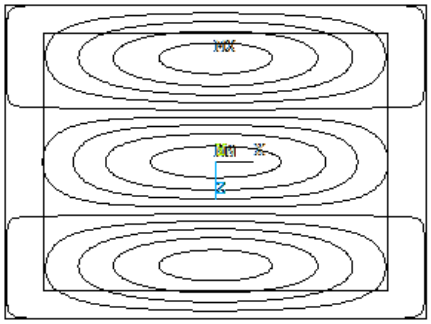

6th mode (110.96Hz)

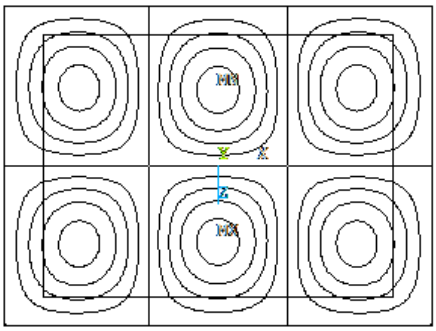

7th mode (117.24 Hz)

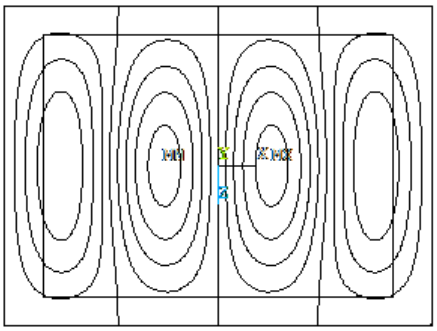

8th mode (135.29 Hz)

Fig. 16 Continued

5. Conclusions

Natural frequencies of a perforated plate with a triangular penetration pattern are obtained by finite element method with respect to ligament efficiency and they are used to extract the effective modulus of elasticity. The effective modulus of elasticity of the fully perforated plate is applied to the modal analysis of a partially perforated rectangular plate using a homogeneous finite element model. The natural frequencies and the corresponding mode shapes of the homogeneous model are compared with those of the detailed finite element model of the partially perforated rectangular plate in order to check the validity of the effective modulus of elasticity. In addition, theoretical method to calculate the natural frequencies of a partially perforated rectangular plate is suggested according to the Rayleigh-Ritz method, and its results are also compared to those from the finite element analysis, showing that the suggested effective modulus of elasticity can be applicable to the partially perforated rectangular plate with a triangular penetration pattern with the fixed boundary condition. It will reduce the finite element model size, computation time and storage memory for the dynamic analysis based on the finite element method.

References

ANSYS (2013), ANSYS Structural Analysis Guide, ANSYS, Inc., Houston, USA.

ASME (2007), ASME PVP Code, Section III, Division 1, Appendices, Non-mandatory Appendix A, Article A-8000, Stresses in Perforated Flat Plates.

Cernescu, A., Romanoff, J., Remes, H., Faur, N. and Jelovica, J. (2014), "Equivalent mechanical properties for cylindrical cell honeycomb core structure", *Compos. Struct*., **108**, 866-875.
Chang, Y.S., Jhung, M.J., Lee, B.S., Kim, H.S. and Hur, N.S. (2013), *Structural Integrity of Nuclear Components*, Hanshouse, Seoul, Korea.
Cupial, P. (1997), "Calculation of the natural frequencies of composite plates by the Rayleigh–Ritz method with orthogonal polynomials", *J. Sound Vib.*, **201**(3), 385-387.
Grimes, R.G., Lewis, J.G. and Simon, H.D. (1994), "A Shifted Block Lanczos Algorithm for Solving Sparse Symmetric Generalized Eigenproblems", *SIAM J. Mat. Anal. Appl.*, **15**(1), 228-272.
Ilanko, S. and Monterrubio L.E. (2014), *The Rayleigh-Ritz Method for Structural Analysis*, John Wiley & Sons, Inc., Hoboken, NJ, USA.
Jhung, M.J. (1997), "Axial Response of PWR fuel assemblies for earthquake and pipe break excitations", *Struct. Eng. Mech.*, **5**(1), 149-165.
Jhung, M.J. and Jeong, K.H. (2015), "Free vibration analysis of perforated plate with square penetration pattern using equivalent material properties", *Nucl. Eng. Tech.*, **47**(4), 500-511.
Kerboua, Y., Lakis, A.A., Thomas, M. and Marcouiller, L. (2008), "Computational modeling of coupled fluid-structure systems with applications", *Struct. Eng. Mech.*, **29**(1), 91-111.
Kim, D.H, Chang, Y.S. and Jhung, M.J. (2014), "Numerical study on fluid flow by hydrodynamic loads in reactor internals", *Struct. Eng. Mech.*, **51**(6), 1005-1016.
Ko, D.Y. and Kim, K.H. (2013), "Structural analysis of CSB and LSS for APR1400 RVI CVAP", *Nucl. Eng. Des.*, **261**, 76-84.
Li, R.C. and Zhang, L.H. (2013), *Convergence of Block Lanczos Method for Eigenvalue Clusters*, University of Texas, Arlington, USA.
O'Donnell, W. J. (1973), "Effective elastic constants for the bending of thin perforated plates with triangular and square penetration patterns", *J. Eng. Indus.*, **95**, 121-128.
Slot, T. and O'Donnell, W.J. (1971), "Effective elastic constants for thick perforated plates with triangular and square penetration patterns", *J. Eng. Indus.*, **93**(4), 935-942.

CC